ANZIAM J. **65** (2023), 248–272
doi:10.1017/S1446181123000196

NONLINEAR SELF-MODULATION OF GRAVITY-CAPILLARY WAVES ON SHEAR CURRENTS IN FINITE DEPTH

TANMOY PAL[1] and ASOKE KUMAR DHAR[1]✉

(Received 5 May, 2023; accepted 10 October, 2023; first published online 12 January, 2024)

Abstract

A nonlinear evolution equation correct to fourth order is developed for gravity-capillary waves on linear shear currents in finite water depth. Therefore, this equation covers both effects of depth uniform currents and uniform vorticity. Starting from this equation, an instability analysis is then made for narrow banded uniform Stokes waves. The notable feature is that our investigation due to fourth order shows a remarkable improvement compared with the third-order one, and produces an excellent result compatible with the exact result of Longuet-Higgins. We observe that linear shear currents considerably change the modulational instability properties of capillary-gravity waves, such as the growth rate and bandwidth of instability.

2020 *Mathematics subject classification*: primary 76B07; secondary 76B15, 76B45.

Keywords and phrases: nonlinear Schrödinger equation, gravity-capillary waves, modulational instability, linear shear current.

1. Introduction

Generally, in coastal and ocean waters, the velocity profiles are typically established by bottom friction and surface stress due to the wind, and so the velocity profiles change with water depth. Currents produce shear at the bottom of the ocean, namely ebb, and flood currents caused by tides may have a significant influence on water waves. In any region where the wind is flowing, there is a surface drift of the water, and water waves are particularly responsive to the velocity in the upper layer. Capillary waves are usually generated by the wind, which also produces a shear flow in the upper layer of the water so that the capillary waves move in the presence of vorticity. These short waves play a significant role in the subsequent development of wind-generated gravity-capillary waves (GCWs), contribute to some extent to the ocean surface stress and consequently participate in air–ocean momentum transfer. Therefore, an accurate

[1]Department of Mathematics, Indian Institute of Engineering Science and Technology, Shibpur, Howrah 711103 West Bengal, India; e-mail: tpal2966@gmail.com, asoke.dhar@gmail.com
© The Author(s), 2024. Published by Cambridge University Press on behalf of Australian Mathematical Publishing Association Inc.

https://doi.org/10.1017/S1446181123000196 Published online by Cambridge University Press

representation of the surface stress is important in modelling and forecasting ocean wave dynamics.

As waves nearly always coexist with currents in the sea, nonlinear wave–current interactions attract the attention of many scientists to carry out research in hydrodynamics and ocean engineering. It is well known that currents can considerably alter the characteristics of surface waves [2, 20, 25, 35]. Preceding studies have established that the interactions between waves and currents are mainly dependent on the direction of propagation and the vertical distribution of currents [17, 23, 35]. There are many situations where currents are vertically sheared. Illustrations include wind-driven currents and ebb flow at a river mouth [29, 27]. So the effect of vertical vorticity should be considered in the wave–current interaction.

Surface water waves moving steadily on a rotational current have been analysed by several authors, namely, Tsao [40], Dalrymple [7], Brevik [3], Simmen and Saffman [37], Teles Da Silva and Peregrine [38], Pak and Chow [34], Kishida and Sobey [21], Constantin [6] and so forth. Johnson [19] investigated the modulation of a two-dimensional harmonic plane waves travelling in the presence of arbitrary vorticity, but did not discuss elaborately the instability analysis as a function of the vorticity and water depth. The modulational instability analysis of weakly nonlinear waves with current shear was made by Oikawa et al. [30]. Choi [5] also studied the modulational instability of gravity waves on shear currents. For fixed wave steepness, he then compared his findings in the case of irrotational motion and observed that the envelope of the modulated wave grows faster for positive shear current and slower for negative shear current. Okamura and Oikawa [31] numerically studied the instability properties of two-dimensional Stokes waves on a linear shear current to three-dimensional small rotational disturbances. A nonlinear Schrödinger equation (NLSE) for periodic gravity waves on deep water that includes an inhomogeneous current with horizontal shear was derived by Hjelmervik and Trulsen [13]. Using this equation for Monte Carlo simulations, they investigated the effect of nonlinearity with respect to the variation of significant wave height, kurtosis and occurrence of freak waves.

Thomas et al. [39] developed a third-order NLSE for surface gravity waves on arbitrary water depth in the presence of constant vorticity, and presented the importance of the coupling between the mean flow response and the vorticity. Hsu et al. [16] then elaborated that paper to include capillarity, and studied both the effects of vorticity and capillarity on modulational instability. Later, Dhar and Kirby [9] derived a fourth-order nonlinear evolution equation (NLEE) for GCWs on finite depth with constant vorticity. From the studies on vorticity modified NLSEs of preceding authors, it is revealed that they considered only the effect of vorticity. In fact, vortices usually occur in combination with depth-uniform currents. Therefore, it is necessary to derive an equation which includes both the effects of depth-uniform currents and vorticity. Keeping this point in view, Liao et al. [22] derived a linear shear current modified NLSE correct to third order on arbitrary water depth and showed that shear currents play an important role in modulational instability properties of weakly nonlinear plane waves, such as the growth rate of instability and bandwidth.

https://doi.org/10.1017/S1446181123000196 Published online by Cambridge University Press

Dysthe [11] reported that the fourth-order NLEE is an excellent starting point for analysing the nonlinear effects of surface waves in deep water. Therefore, according to Dysthe [11], one avenue of interest is to combine higher-order terms in the third-order NLEE, and the purpose of this paper is to develop a higher-order NLEE and to investigate a theory for GCWs on linear shear current in finite water depth. The new fourth-order outcome shows a remarkable modification in the instability behaviour from the third-order one in deep water. This paper is an extension of the paper by Dhar and Kirby [9] to include the effect of depth uniform current on modulational instability properties.

The paper is structured as follows. In Section 2, the basic equations for the problem are given. In Section 3, we develop a fourth-order NLEE for GCWs on linear shear current in a finite depth of water. We present the evolution equation for deep water and discuss the coupling between the mean flow term and the current shear in Section 4. Next, we make the modulational instability analysis of a uniform wave train in Section 5 and finally, conclusions with results are given in Section 6.

2. Basic equations

Consider the equation of the undisturbed free surface as the $y = 0$ plane. Here, we take two-dimensional Cartesian coordinates x, y in which the x-axis is directed towards the direction of propagation of the waves and the y-axis is oriented upwards. We suppose that the fluid motion is incompressible and nonviscous and the waves are moving steadily on a vertical linear shear current, which can be separated into a depth uniform current v and a uniform vorticity $-\omega$. Let $y = \eta(x, t)$ be the equation of the free surface in the perturbed state. There is a potential function $\phi(x, y, t)$ for which the total velocity $\mathbf{u}$ of the fluid flow can be represented as

$$\mathbf{u}(x, y) = (v + \omega y)\mathbf{i} + \nabla\phi(x, y, t),$$

where v is the speed of the linear shear current along the direction of propagation of the waves at the free surface and $\mathbf{i}$ represents the unit vector along the x-axis. As the vorticity $-\omega$ of the basic flow is constant, the velocity field induced by a two-dimensional perturbation must be irrotational due to Kelvin's theorem [39].

As the perturbation is supposed to be potential, the perturbed velocity potential ϕ and the stream function ψ of the fluid satisfy the two-dimensional Laplace equations as follows:

$$\nabla^2\phi = 0, \quad \nabla^2\psi = 0, \quad \text{in } -d < y < \eta(x, t), \tag{2.1}$$

in which ϕ, ψ are connected by the Cauchy–Riemann relations

$$\frac{\partial\phi}{\partial x} = \frac{\partial\psi}{\partial y}, \quad \frac{\partial\phi}{\partial y} = -\frac{\partial\psi}{\partial x}.$$

https://doi.org/10.1017/S1446181123000196 Published online by Cambridge University Press

The kinematic free surface boundary condition is

$$\frac{\partial \phi}{\partial y} - \frac{\partial \eta}{\partial t} - v\frac{\partial \eta}{\partial x} = \left(\frac{\partial \phi}{\partial x} + \omega\eta\right)\frac{\partial \eta}{\partial x}, \quad \text{on } y = \eta(x,t). \tag{2.2}$$

The dynamic surface boundary condition is given by

$$\frac{\partial \phi}{\partial t} + v\frac{\partial \phi}{\partial x} - \omega\psi + g\eta = -\frac{1}{2}(\nabla\phi)^2 - \omega\eta\frac{\partial \phi}{\partial x} + \left(\frac{T}{\rho}\right)\frac{\eta_{xx}}{(1+\eta_x^2)^{3/2}}, \quad \text{on } y = \eta(x,t), \tag{2.3}$$

where T and ρ denote the surface tension coefficient and density of bulk water, respectively.

Also at the bottom, ϕ and ψ satisfy the following boundary conditions:

$$\frac{\partial \phi}{\partial y} = 0, \quad \psi = 0, \quad \text{on } y = -d. \tag{2.4}$$

We consider the solutions of equations (2.1)–(2.4) as follows:

$$G = G_0 + \sum_{m=1}^{\infty}[G_m \exp\{im(kx - \sigma t)\} + \text{c.c.}], \tag{2.5}$$

where G stands for $\phi(x,y,t)$, $\psi(x,y,t)$ and the free surface elevation $\eta(x,t)$, k and σ represent carrier wavenumber and frequency respectively and c.c. means complex conjugate. Here ϕ_0, ϕ_m, ϕ_m^*, ψ_0, ψ_m, ψ_m^* $(m = 1, 2, \ldots)$ are slowly varying functions of $x_1 = \epsilon x$, $t_1 = \epsilon t$, y ; η_0, η_m, η_m^* $(m = 1, 2, \ldots)$ are functions of x_1, t_1. Here, ϵ is a slow ordering parameter which measures the weakness of nonlinearity and $0 < \epsilon << 1$.

The linear dispersion relation to determine the frequency σ of the carrier wave is

$$f(\sigma, k) \equiv \sigma^2(1-\overline{v})(1-\overline{v}+\beta) - gk\mu(1+\kappa) = 0,$$

where $\overline{v} = v/c$, $c = \sigma/k$, the velocity of the carrier wave, $\beta = \mu\overline{\omega}$, $\overline{\omega} = \omega/\sigma$, $\mu = \tanh p$, $p = kd$, $\kappa = Tk^2/\rho g$.

The group velocity c_g becomes

$$c_g = c\{(1-\overline{v})^2 p(1-\mu^2)/\mu + (1-\overline{v})(1-\overline{v}+\beta)(1+3\kappa)/(1+\kappa) + \overline{v}(2-2\overline{v}+\beta)\}(2-2\overline{v}+\beta)^{-1}.$$

3. Derivation of evolution equation using multiple scale method

In this section, we develop an NLEE accurate up to fourth order for narrow banded GCWs in the case of finite water depth, and discuss the two types of singularity.

On substituting the expansions in equation (2.5) into equation (2.1) and using bottom conditions in equation (2.4), we get the required solutions for ϕ_m, ψ_m, $(m = 1, 2)$ as follows:

https://doi.org/10.1017/S1446181123000196 Published online by Cambridge University Press

$$\phi_m = \frac{\cosh\left((y+d)K_m\right)}{\cosh\left(dK_m\right)} C_m,$$
$$\psi_m = \frac{\sinh\left((y+d)K_m\right)}{\cosh\left(dK_m\right)} D_m, \tag{3.1}$$

where $K_m = km - i\epsilon(\partial/\partial x_1)$ and $C_m,\ D_m$ are functions of x_1 and t_1. Next, for $m = 0$,

$$\overline{\phi}_0 = \frac{\cosh\left((y+d)\epsilon\overline{k}\right)}{\cosh\left(\epsilon d\overline{k}\right)} \overline{C}_0,$$
$$\overline{\psi}_0 = \frac{\sinh\left((y+d)\epsilon\overline{k}\right)}{\cosh\left(\epsilon d\overline{k}\right)} \overline{D}_0, \tag{3.2}$$

in which $\overline{C}_0,\ \overline{D}_0$ are functions of $\overline{k},\ \overline{\omega}_1$, and $\overline{\phi}_0,\ \overline{\psi}_0$ are Fourier transforms of $\phi_0,\ \psi_0$, respectively, given by

$$(\overline{\phi}_0, \overline{\psi}_0) = \frac{1}{2\pi} \iint_{-\infty}^{\infty} (\phi_0, \psi_0) \exp[-i(\overline{k}x_1 - \overline{\omega}_1 t_1)]\, dx_1\, dt_1.$$

Inserting the expansions in equation (2.5) into the Taylor's expanded form of equations (2.2) and (2.3) about $y = 0$ and then equating coefficients of exp $im(kx - \sigma t)$, for $m = 1, 2, 0$ on both sides, we obtain three sets of equations into each of which we substitute the solutions for $\phi_m,\ \psi_m$ given by equations (3.1)–(3.2). For the purpose of solving these equations, we take the expansions as follows:

$$H_m = \sum_{n=1}^{\infty} \epsilon^n H_{mn}\ (m = 0, 1), \quad H_2 = \sum_{n=2}^{\infty} \epsilon^n H_{2n}, \tag{3.3}$$

where H_p stands for $C_p,\ D_p$ and η_p $(p = 0, 1, 2)$.

Inserting equation (3.3) into the three sets of equations and then equating coefficients of several powers of ϵ, we get a sequence of equations. From the first (lowest) and second-order equations of the three sets, we get solutions for $(C_{11},\ C_{12})$, $(C_{22},\ \eta_{22},\ C_{23},\ \eta_{23})$ and $(C_{01},\ \eta_{01},\ C_{02},\ \eta_{02})$, respectively.

The equation corresponding to equation (2.3) of the first set of equations can be put in the following convenient form:

$$f(\sigma_1, K_1)\eta_1 = -i\{(\sigma_1 - K_1 v) + \omega\mu\}a_1 - K_1\mu b_1, \tag{3.4}$$

where $\sigma_1 = \sigma + i\epsilon(\partial/\partial t_1),\ K_1 = k - i\epsilon(\partial/\partial x_1)$ and $a_1,\ b_1$ are obtained from nonlinear terms.

We retain terms up to fourth-order $O(\epsilon^4)$ and insert solutions for different perturbed quantities arising on the right-hand side of equation (3.4). Finally, applying the transformations

$$\xi = \epsilon(x - c_g t), \quad \tau = \epsilon^2 t, \tag{3.5}$$

https://doi.org/10.1017/S1446181123000196 Published online by Cambridge University Press

and taking $\eta = \eta_1 = \epsilon\eta_{11} + \epsilon^2\eta_{12}$, we get the fourth-order NLEE as follows:

$$i\frac{\partial\eta}{\partial\tau} + \alpha_1\frac{\partial^2\eta}{\partial\xi^2} + i\alpha_2\frac{\partial^3\eta}{\partial\xi^3} = \mu_1 \mid \eta \mid^2 \eta + i\mu_2 \mid \eta \mid^2 \frac{\partial\eta}{\partial\xi} + i\mu_3\eta^2\frac{\partial\eta^*}{\partial\xi} + \mu_4\eta\frac{\partial}{\partial\xi}F^{-1}\left[\frac{F\frac{\partial}{\partial\xi}(\mid \eta \mid^2)}{\bar{k}\tanh(\epsilon\bar{k}p)}\right], \tag{3.6}$$

where F represents the spatial Fourier transform. The coefficients α_1, α_2 and $\mu_i (i = 1, 2, 3, 4)$ are given in Appendix A.

We have applied the scaling transformations $\eta' = 2k\eta$, $\xi' = k\xi$, $\tau' = \sigma\tau$ in equation (3.6) and then dropped the primes. The nonlinear spatio-temporal evolution of weakly nonlinear GCWs can be described by the NLEE in equation (3.6), provided the wave steepness is small ($\ll 1$) and the spectral bandwidth is narrow ($\ll 1$).

Note that the derivation of the NLEE correct to fourth order involves some algebra. To render the results convincing, it is useful to compare with other results.

We can check that the coefficients α_1 and μ_1 corresponding to cubic NLEE reduce to those of Liao et al. [22] for $\kappa = 0$ and to those of Hsu et al. [16] for $\overline{\nu} = 0$.

In the expression for μ_1, due to the presence of the factor

$$\mu^2(1 - \overline{\nu}) - \kappa\{(3 - \mu^2)(1 - \overline{\nu}) + 3\beta\}$$

in its denominator resulting from the expression for η_{22}, the NLEE in equation (3.6) does not remain valid when κ satisfies equation (3.7). The value of κ for which the singularity occurs is

$$\kappa = \frac{\mu^2(1 - \overline{\nu})}{(3 - \mu^2)(1 - \overline{\nu}) + 3\beta}. \tag{3.7}$$

Herein, the speeds c of the carrier wave and second harmonic wave coincide (for clarification, see [28]), resulting in the phenomenon known as second harmonic resonance.

This resonance, also called capillary-gravity resonance, was first pointed out for $\beta = 0$, $\overline{\nu} = 0$ and for deep water by Wilton [41], where $\kappa = 1/2$. The physical significance of the value of $\kappa = 1/2$ was explained by Harrison [12] for deep water. He argued that the effect of nonlinearity on GCWs is completely different depending on whether κ is greater than or less than $1/2$. The effect of nonlinearity (higher harmonics) for $\kappa > 1/2$ is to distort the wave profile, so that the crests are flattened and the troughs are sharpened. Wave profiles of this kind are known as pure capillary waves. A nonlinear effect reverse to this is observed when $\kappa < 1/2$ and profiles of this kind are called gravity waves.

We also get a second possible singularity related to the long/short wave resonance, in which the group velocity of the short wave is equal to the phase velocity of the long wave. The last term within the brackets of the expression for μ_1 (see Appendix A) corresponds to the coupling between the wave induced mean flow response and the

https://doi.org/10.1017/S1446181123000196 Published online by Cambridge University Press

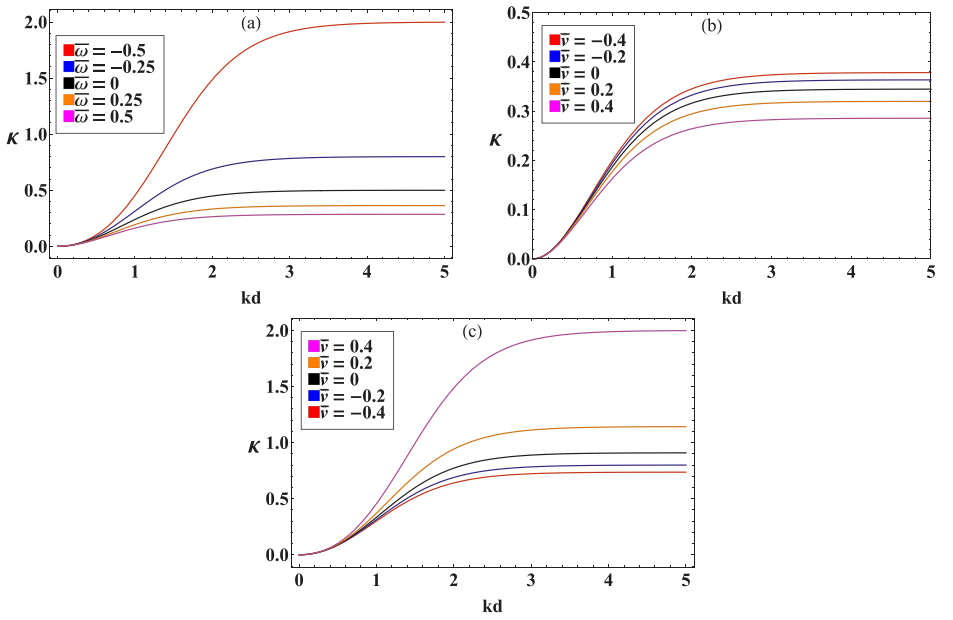

FIGURE 1. Behaviour of κ against kd: (a) $\overline{v} = 0$ and different values of $\overline{\omega}$; (b) $\overline{\omega} = 0.3$ and different values of $\overline{v}$; (c) $\overline{\omega} = -0.3$ and different values of $\overline{v}$.

vorticity which occurs at third order, and this coupling has a significant impact on modulational instability. This term of μ_1 is found to be singular when

$$(\gamma - \overline{v})(\gamma + \overline{\omega}p) = \frac{(1-\overline{v})(1-\overline{v}+\beta)p}{\mu(1+\kappa)},$$

where $\gamma = c_g/c$, and may be expressed as

$$c_g(c_g + \omega d) = gd \quad \text{for } \overline{v} = 0. \tag{3.8}$$

Equation (3.8) reduces to $c_g^2 = gd$ in the absence of vorticity, which corresponds to a long wave resonance found by Davey and Stewartson [8], and Djordjevic and Redekopp [10].

We have plotted the critical surface tension coefficient κ given by equation (3.7) as a function kd in Figure 1 for some values of $\overline{v}$ and $\overline{\omega}$. It is found that the value of κ decreases with the increase of negative vorticity ($\overline{\omega} > 0$) and eventually, the influence of capillarity is lost. Again, the value of κ increases with the increase of positive vorticity ($\overline{\omega} < 0$), and the influence of capillarity is expected to become important. Further, we observe that for a fixed value of negative vorticity, the depth uniform following current decreases the value of κ, while the reverse current increases it. The effect reverse to this is found in the case of positive vorticity. The curve drawn in Figure 1(a) for $\overline{v} = 0$ and $\overline{\omega} = 0$ is identical to the curve in figure 2(a) of Hsu et al. [15].

https://doi.org/10.1017/S1446181123000196 Published online by Cambridge University Press

4. Evolution equation for deep water and nonlinear coupling

Herein, we first reduce the evolution equation for deep water, and then discuss the coupling due to nonlinearity between the wave-induced mean flow term and the vorticity, which occurs at both third and fourth orders. The infinite depth approximation is $\mu = \tanh p \to 1$. Further, if $\tanh(\epsilon\bar{k}p) \to 1$ (with $p = kd$) is used in the last term of equation (3.6), then it takes the form

$$\tilde{\mu}_4\eta\frac{\partial}{\partial\xi}F^{-1}\left[\frac{F\frac{\partial}{\partial\xi}(|\eta|^2)}{\bar{k}}\right] = \tilde{\mu}_4\eta H\left[\frac{\partial}{\partial\xi}(|\eta|^2)\right],$$

in which H is the Hilbert transform operator given by

$$H[\Gamma(\xi)] = \frac{1}{\pi}P\int_{-\infty}^{\infty}\frac{\Gamma(\xi')}{\xi'-\xi}\,d\xi'.$$

Now equation (3.6) for deep water can be written as

$$i\frac{\partial\eta}{\partial\tau} + \tilde{\alpha}_1\frac{\partial^2\eta}{\partial\xi^2} + i\tilde{\alpha}_2\frac{\partial^3\eta}{\partial\xi^3} = \tilde{\mu}_1|\eta|^2\eta + i\tilde{\mu}_2|\eta|^2\frac{\partial\eta}{\partial\xi} + i\tilde{\mu}_3\eta^2\frac{\partial\eta^*}{\partial\xi} + \tilde{\mu}_4\eta H\left[\frac{\partial}{\partial\xi}(|\eta|^2)\right], \tag{4.1}$$

where the coefficients for deep water are given in Appendix B. Without vorticity and depth uniform current $\bar{v}$, these coefficients agree with those of Hogan [14].

At third order, the coefficient $\tilde{\mu}_1$ of equation (4.1) contains two terms. The first term is obtained from the dispersion relation of GCWs propagating on a linear shear current, and the second term arises from the nonlinear coupling between the wave-induced mean flow response and the vorticity. Without vorticity, it is to be noted that this coupling disappears. Again, for $\beta = 0$ and $\bar{v} = 0$, the third-order nonlinear coefficient $\tilde{\mu}_1$ vanishes when $\omega = -2/3$ and equation (4.1) contains only fourth-order nonlinear terms. At fourth order, the coefficient $\tilde{\mu}_4$ arises from a nonlinear coupling between wave-induced current and the wave field, and this coupling is still present when $\omega = 0$, as found a long time ago by Dysthe [11]. The significant effect introduced to fourth order is the wave-induced mean flow response to nonuniformities in the radiation stress caused by modulation of the finite amplitude wavetrain, as reported by Dysthe [11].

5. Modulational instability analysis and results

On the basis of the NLEE for deep water, we investigate here the influence of linear shear current on the modulational instability and obtain the nonlinear dispersion relation and the instability condition.

The solution for the uniform wavetrain of equation (4.1) is

$$\eta = \eta_0\exp(i\Delta\sigma\tau),$$

https://doi.org/10.1017/S1446181123000196 Published online by Cambridge University Press

where η_0 is the wave steepness and the nonlinear frequency shift $\Delta\sigma$ is given by

$$\Delta\sigma = -\tilde{\mu}_1\eta_0^2.$$

We next introduce the following small perturbation in the above solution:

$$\eta = \eta_0[1 + \eta'(\xi, \eta)]\exp(i\Delta\sigma\tau). \tag{5.1}$$

We substitute equation (5.1) in equation (4.1), linearize with respect to η' and $\eta^{*\prime}$, and separate the equations after setting $\eta' = \eta'_r + i\eta'_i$, where η'_r and η'_i are real. Then we take the Fourier transform of these equations defined by

$$(\overline{\eta}'_r, \overline{\eta}'_i) = \int_{-\infty}^{\infty} (\eta'_r, \eta'_i)\exp(-i\lambda\xi)\, d\xi,$$

and obtain two equations

$$\left[\frac{\partial}{\partial\tau} - i(\tilde{\alpha}_2\lambda^3 + \eta_0^2\tilde{\mu}_2\lambda - \eta_0^2\tilde{\mu}_3\lambda)\right]\overline{\eta}'_i + [\tilde{\alpha}_1\lambda^2 + 2\eta_0^2\tilde{\mu}_1 - 2\eta_0^2\tilde{\mu}_4 \mid \lambda \mid]\overline{\eta}'_r = 0$$

and

$$\tilde{\alpha}_1\lambda^2\overline{\eta}'_i - \left[\frac{\partial}{\partial\tau} - i(\tilde{\alpha}_2\lambda^3 + \eta_0^2\tilde{\mu}_2\lambda + \eta_0^2\tilde{\mu}_3\lambda)\right]\overline{\eta}'_r = 0.$$

Assuming τ-dependence of η'_r and η'_i to be of the form $\exp(-i\tilde{\Omega}\tau)$, we get the nonlinear dispersion relation as follows:

$$\tilde{\Omega} = \tilde{\gamma}\lambda - \tilde{\alpha}_2\lambda^3 - \eta_0^2\tilde{\mu}_2\lambda \pm \sqrt{\tilde{\alpha}_1\lambda^2(\tilde{\alpha}_1\lambda^2 + 2\eta_0^2\tilde{\mu}_1 - 2\eta_0^2\tilde{\mu}_4 \mid \lambda \mid)}, \tag{5.2}$$

where $\tilde{\Omega}$, λ are the perturbed frequency and wave number, respectively.

For instability,

$$\tilde{\alpha}_1(\tilde{\alpha}_1\lambda^2 + 2\eta_0^2\tilde{\mu}_1 - 2\eta_0^2\tilde{\mu}_4 \mid \lambda \mid) < 0, \tag{5.3}$$

and the growth rate $\mathrm{Im}(\tilde{\Omega})$ then becomes

$$\mathrm{Im}(\tilde{\Omega}) = \lambda\sqrt{-\tilde{\alpha}_1(\tilde{\alpha}_1\lambda^2 + 2\eta_0^2\tilde{\mu}_1 - 2\eta_0^2\tilde{\mu}_4 \mid \lambda \mid)}, \tag{5.4}$$

where $\mathrm{Im}(\tilde{\Omega})$ indicates the imaginary part of $\tilde{\Omega}$.

From equation (5.3), the bandwidth of instability becomes

$$\lambda = \sqrt{\frac{-2\tilde{\mu}_1}{\tilde{\alpha}_1}}\eta_0 + \frac{\tilde{\mu}_4}{\tilde{\alpha}_1}\eta_0^2.$$

Again, $\tilde{\Omega}_r$, which is the real part of $\tilde{\Omega}$ at marginal stability, gives

$$\tilde{\Omega}_r = \tilde{\gamma}\left[\sqrt{\frac{-2\tilde{\mu}_1}{\tilde{\alpha}_1}} + \frac{\tilde{\mu}_4}{\tilde{\alpha}_1}\eta_0\right]\eta_0.$$

https://doi.org/10.1017/S1446181123000196 Published online by Cambridge University Press

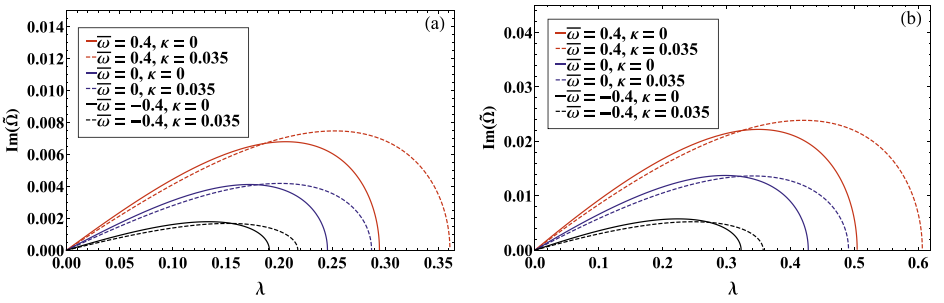

FIGURE 2. Plot of modulational instability growth rate against λ for $\overline{v} = 0$ and several values of $\overline{\omega}$ and κ: (a) $\eta_0 = 0.1$; (b) $\eta_0 = 0.2$.

If the condition in equation (5.3) is satisfied, the maximum growth rate $\tilde{G}_m$ takes the form

$$\tilde{G}_m = \mid \tilde{\mu}_1 \mid \left[1 - \frac{\tilde{\mu}_4}{\tilde{\mu}_1}\sqrt{-\frac{\tilde{\mu}_1}{\tilde{\alpha}_1}}\eta_0\right]\eta_0^2, \tag{5.5}$$

which occurs for wavenumber of perturbation λ_m

$$\lambda_m = \sqrt{\frac{-\tilde{\mu}_1}{\tilde{\alpha}_1}}\eta_0 + \frac{3\tilde{\mu}_4}{4\tilde{\alpha}_1}\eta_0^2.$$

Further, $\tilde{\Omega}_{rm}$, the real part of $\tilde{\Omega}$ corresponding to λ_m takes the form

$$\tilde{\Omega}_{rm} = \tilde{\gamma}\left[\sqrt{\frac{-\tilde{\mu}_1}{\tilde{\alpha}_1}} + \frac{3\tilde{\mu}_4}{4\tilde{\alpha}_1}\eta_0\right]\eta_0. \tag{5.6}$$

Physically, we observe two types of nonlinear interaction influencing the results. First, the relative signs of the frequency dispersion term $\tilde{\alpha}_1\eta_{\xi\xi}$ and the nonlinear term $\tilde{\mu}_1 \mid \eta \mid^2 \eta$ of equation (4.1) that occur at third order govern the overall modulational instability properties of the solution. It is important to note that the key element is the sign of the product $\tilde{\alpha}_1\tilde{\mu}_1$. Second, the corrections to the modulational instability that occur at fourth order come from the nonlinear interaction between the induced mean flow term $\tilde{\mu}_4\eta H[(\partial/\partial\xi)(\mid \eta \mid^2)]$ and the frequency dispersion term $\tilde{\alpha}_1\eta_{\xi\xi}$. Further, significance has been attached to the term $i\tilde{\mu}_2 \mid \eta \mid^2 \eta_\xi$ of equation (4.1). We observe from equation (5.2) that it gives the real $O(\eta_0^2)$ correction to the frequency of very long plane perturbation to the wave train.

Figures 2 and 3 exhibit the influence of vorticity, depth uniform current and capillarity from the fourth-order result on the growth rate of instability given by equation (5.4) in deep water. Herein, the instability growth rate is found to be considerably changed by the magnitude and sign of the current shear. As observed from Figure 2, the current shear for $\overline{\omega} > 0$ tends to increase the growth rate, whereas the current shear for $\overline{\omega} < 0$ has the reverse effect. Figure 3 exhibits that depth uniform reverse currents can spread out the onset criterion and considerably increase the growth

https://doi.org/10.1017/S1446181123000196 Published online by Cambridge University Press

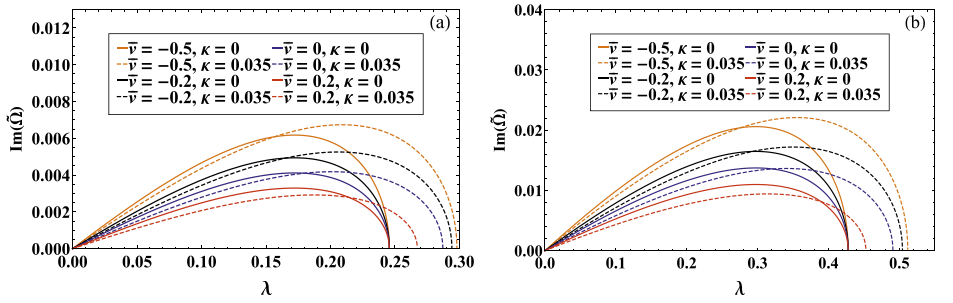

FIGURE 3. Plot of $\mathrm{Im}(\tilde{\Omega})$ as a function of λ for $\overline{\omega} = 0$ and several values of $\bar{\nu}$ and κ: (a) $\eta_0 = 0.1$; (b) $\eta_0 = 0.2$.

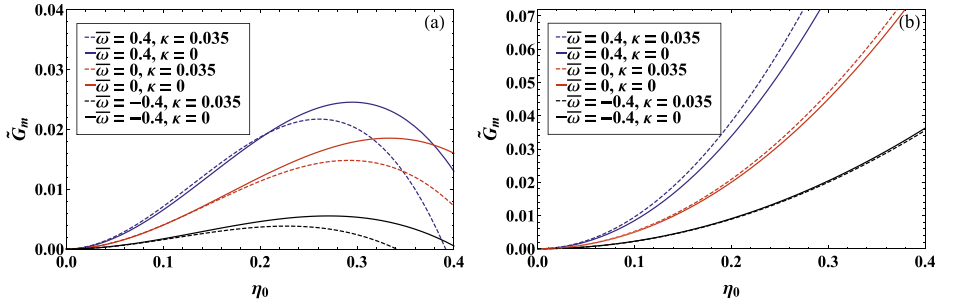

FIGURE 4. Plot of $\tilde{G}_m$ against η_0 for $\bar{\nu} = 0$ and different values of $\overline{\omega}$ and κ: (a) fourth-order result; (b) third-order result.

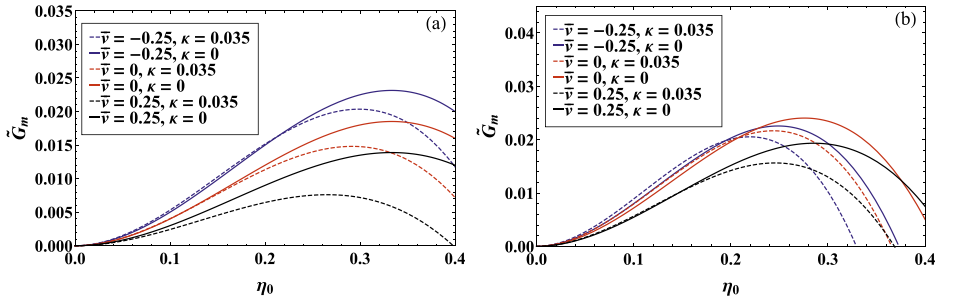

FIGURE 5. Plot of $\tilde{G}_m$ as a function of η_0 for several values of $\bar{\nu}$ and κ: (a) $\overline{\omega} = 0$; (b) $\overline{\omega} = 0.5$.

rate, whereas following currents decrease the growth rate. Furthermore, the effect of capillarity depresses the growth rate giving a stabilizing influence up to a certain value of λ and the growth rate is shown to increase with the increase of η_0.

Using equation (5.5), the maximum growth rate of instability $\tilde{G}_m$ has been drawn in Figures 4 and 5 against η_0 for $\bar{\nu} = 0$ and $\overline{\omega} = 0, 0.5$ respectively. It is observed from Figure 4 that the maximum growth rate obtained from fourth-order results first increases with η_0 and then it diminishes, whereas the maximum growth rate obtained

https://doi.org/10.1017/S1446181123000196 Published online by Cambridge University Press

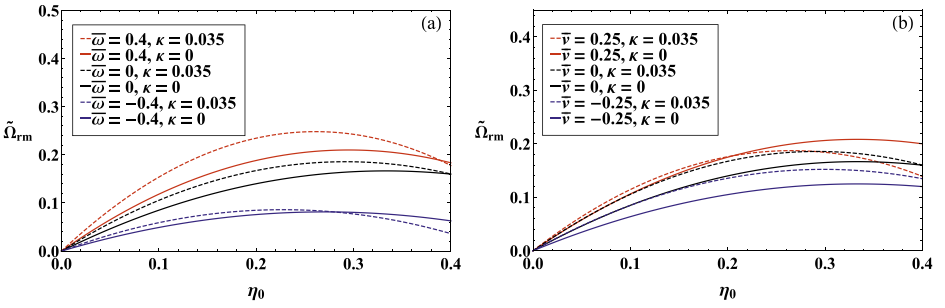

FIGURE 6. Plot of $\tilde{\Omega}_{rm}$ as a function of η_0: (a) $\overline{v} = 0$; (b) $\overline{\omega} = 0$.

from third-order results increases steadily with η_0. Further, the maximum growth rate increases with $\overline{\omega}$ and it decreases with the increase of depth uniform current $\overline{v}$. The curve corresponding to $\overline{v} = 0$, $\overline{\omega} = 0$, $\kappa = 0$ is the same as the curve found in figure 2 of Dysthe [11], and he reported that equation (5.5) for $\overline{v} = 0$, $\overline{\omega} = 0, \kappa = 0$ is considerably close to the exact findings of Longuet-Higgins [24, 25] for $\eta_0 < 0.3$. Thus, we get an excellent agreement with the findings obtained by Longuet-Higgins [24, 25].

The plot of $\tilde{\Omega}_{rm}$ given by equation (5.6) has been depicted against η_0, as shown in Figure 6. From Figure 6(a), we find that the curve obtained from the results for $\overline{v} = 0$, $\overline{\omega} = 0$ and $\kappa = 0$ is the same as that obtained in figure 3 of Dysthe [11]. This particular curve, as indicated by Dysthe, is in good agreement with the curve found from the exact findings of Longuet-Higgins [24, 25], and the experimental results of Lake and Yuen [42] and Benjamin and Feir [1] for $\eta_0 < 0.2$.

5.1. Instability growth rate and bandwidth for finite depth Note that the last term of equation (3.6) contains a term $\tanh(\epsilon\overline{k}p)$. In accordance with Brinch-Nielsen and Jonsson [4], the arbitrary water depth supposition is $\tanh(\epsilon\overline{k}p) = \epsilon\overline{k}kd$, and they have noted that fourth-order terms of equation (3.6) do not contribute to the expression for Im(Ω), where Ω represents the perturbed frequency for finite water depth.

To obtain the growth rate Im(Ω) for finite depth, we replace $\tilde{\alpha}_1$ and $\tilde{\mu}_1$ by α_1 and μ_1, respectively, in equation (5.4), where α_1 and μ_1 are the coefficients of third-order dispersive and nonlinear terms, respectively, of equation (3.6). Thus, at third order, the normalized growth rate becomes

$$\frac{\mathrm{Im}(\Omega)}{\eta_0^2} = \frac{\lambda}{\eta_0}\sqrt{-\alpha_1\left\{\alpha_1\left(\frac{\lambda}{\eta_0}\right)^2 + 2\mu_1\right\}}, \tag{5.7}$$

and the instability bandwidth is

$$\lambda = \sqrt{\frac{-2\mu_1}{\alpha_1}}\eta_0. \tag{5.8}$$

https://doi.org/10.1017/S1446181123000196 Published online by Cambridge University Press

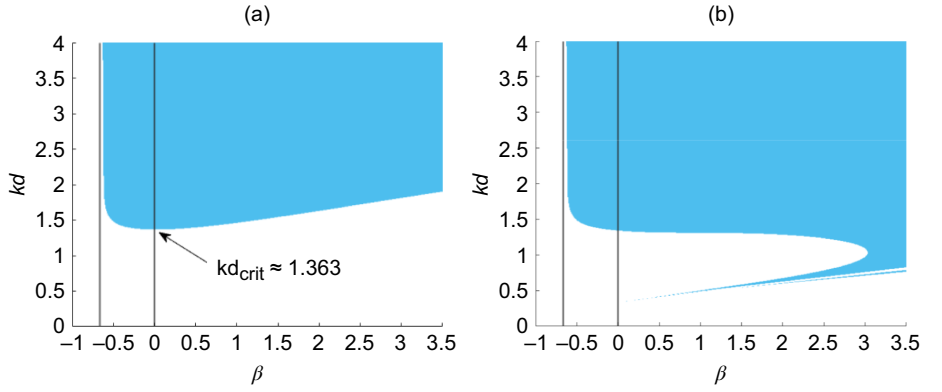

FIGURE 7. Instability diagrams in the (β, kd) plane for $\overline{\nu} = 0$: (a) $\kappa = 0$; (b) $\kappa = 0.035$. The unstable regions are in blue while the stable regions are in white (colour available online).

Further, the maximal growth rate of instability G_m becomes

$$G_m = |\mu_1|\eta_0^2. \tag{5.9}$$

For $\overline{\nu} = 0$, the expressions of $\mathrm{Im}(\Omega)$ and G_m reduce to the corresponding expressions of Hsu et al. [16].

The instability diagrams are shown in Figure 7 as a function of the parameters β and kd for $\kappa = 0$ and 0.035. For $\kappa = 0$, this diagram is identical to figure 3 of Thomas et al. [39]. The critical water depth kd_{crit} of kd for $\beta = 0$ has the well-known value of 1.363, above which the instability prevails. For finite depth, the condition $\alpha_1\mu_1 < 0$ corresponds to modulational instability. For $\overline{\omega} = -2/3$, $\alpha_1\mu_1$ alters sign and, as a consequence, the nature of stability changes. Hence, in deep water, there is no instability when $-1 < \overline{\omega} \leq -2/3$.

Stable and unstable regions are plotted in Figure 8 for $\omega = 0$, $\overline{\nu} = 0$. The red and black curves (online) are due to the singularities in the nonlinear coefficient μ_1. For $\omega = 0$, $\overline{\nu} = 0$, results for instability boundaries are presented by Djordjevic and Redekopp [10], and exhibited in figure 6 of Hsu et al. [16], and our stability diagram matches the findings of Djordjevic and Redekopp [10]. Thus, we can check that this limiting case is again produced correctly.

The effect of negative vorticity ($\omega > 0$) is shown in Figure 9 for $\overline{\nu} = 0$. The red and black curves correspond to the singularities of μ_1. It is found that the vorticity has a considerable effect on the instability diagram of GCWs. With the increase of ω, the instability band along the kd-axis that corresponds to small values of κ becomes narrower.

In Figures 10 and 11, the growth rate $\mathrm{Im}(\Omega)/\eta_0^2$ given by equation (5.7) against λ/η_0 has been plotted for $\overline{\nu} = 0$, and some values of $\overline{\omega}$ and κ for finite depth and deep water, respectively. From Figure 10, one can observe that for finite depth, the growth rate increases notably due to the combined effect of vorticity and capillarity when $\overline{\omega} > 0$,

https://doi.org/10.1017/S1446181123000196 Published online by Cambridge University Press

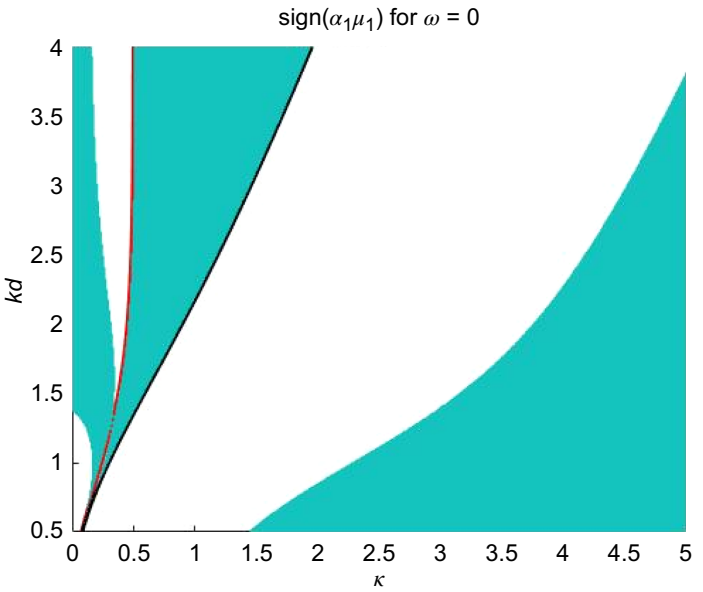

FIGURE 8. Instability diagram in the (kd, κ) plane for $\omega = 0$, $\bar{v} = 0$. The unstable regions are in cyan while the stable regions are in white. The red curve is due to the singularity in μ_1 obtained from the second harmonic resonance given by equation (3.7) and the black curve is due to the singularity in μ_1 obtained from the long wave resonance condition given by equation (3.8) (colour available online).

consistent with the results of Hsu et al. [16]. As observed in these figures for $\kappa = 0$, as shown by Liao et al. [22] and Thomas et al. [39], the current shear for $\overline{\omega} > 0$ tends to significantly enhance the modulational instabilities, whereas the current shear for $\overline{\omega} < 0$ has the adverse effect. Again, the growth rate increases with the increase of water depth.

The plots of $\mathrm{Im}(\Omega)/\eta_0^2$ as a function of λ/η_0 for $\overline{\omega} = 0$ and 0.5 in finite depth are shown in Figures 12 and 13, respectively. It is found that the growth rate increases with the increase of depth uniform opposing current.

Figure 14 shows that in deep water, depth uniform reverse currents significantly increase the growth rate, whereas following currents decrease the modulational instability, consistent with the findings in figure 4(b) of Liao et al. [22] for $\overline{\omega} = 0$, $\kappa = 0$.

In Figure 15, the growth rate $\mathrm{Im}(\Omega)/\eta_0^2$ in quiescent water has been drawn at different water depths kd and two values of κ. The curve for $kd = 1.37$ indicates that the instability vanishes as kd tends to 1.363, which is compatible with the celebrated classical theory. It is observed that the growth rate increases with water depth, compatible with the previous results of Ma et al. [26] and Sedletsky [36].

The maximum growth rate G_m given by equation (5.9) at different water depths kd against η_0 is plotted for $\bar{v} = 0$ and $\overline{\omega} = 0$ in Figures 16 and 17, respectively. From Figure 16, we find that the maximum growth rate increases with $\overline{\omega}$ and Figure 17

https://doi.org/10.1017/S1446181123000196 Published online by Cambridge University Press

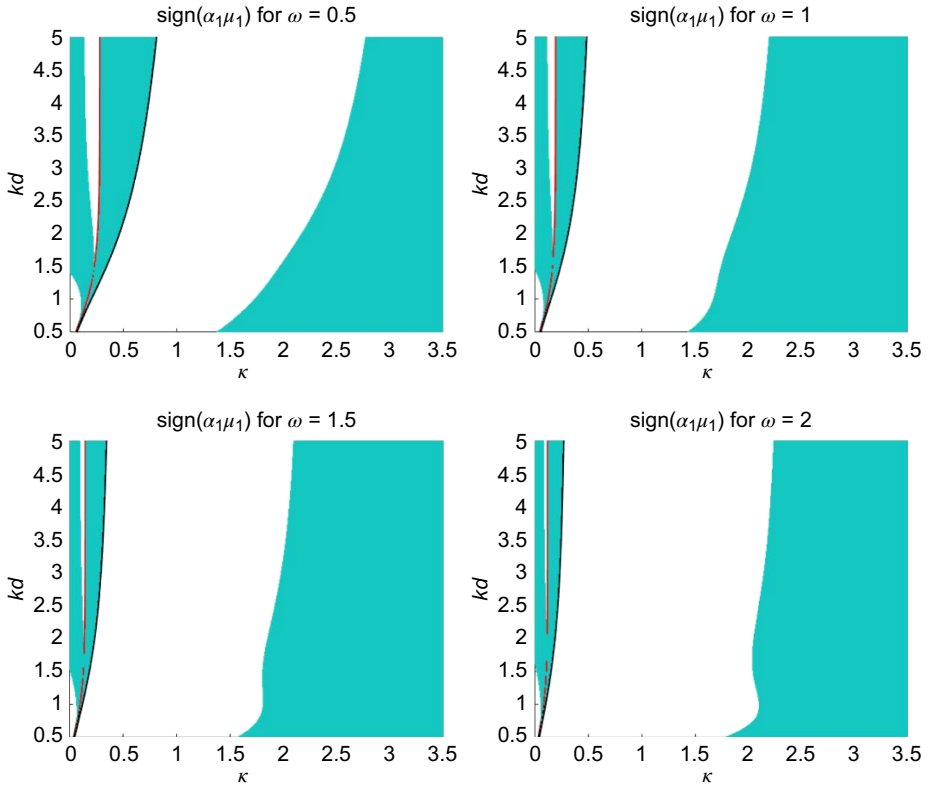

FIGURE 9. Instability diagrams in the (kd, κ) plane for $\overline{\nu} = 0$ and several values of ω. The unstable regions are in cyan while the stable regions are in white (colour available online).

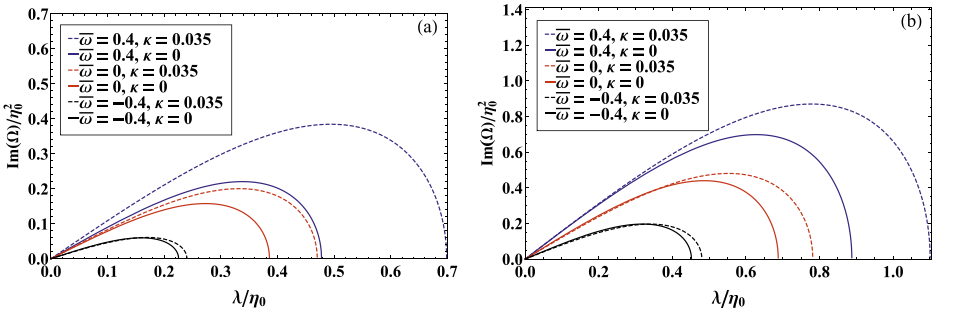

FIGURE 10. Plot of $\mathrm{Im}(\Omega)/\eta_0^2$ as a function of λ/η_0 for $\overline{\nu} = 0$ and several values of $\overline{\omega}$ and κ: (a) $kd = 1.5$; (b) $kd = 2$.

shows that depth uniform reverse currents increase the maximum growth rate, whereas following currents decrease the growth rate.

Next, in Figures 18 and 19, the ratio of the maximum growth rate G_m to its value without shear currents is drawn against $\overline{\omega}$ and $\overline{\nu}$, respectively. In Figure 18, graphs are

https://doi.org/10.1017/S1446181123000196 Published online by Cambridge University Press

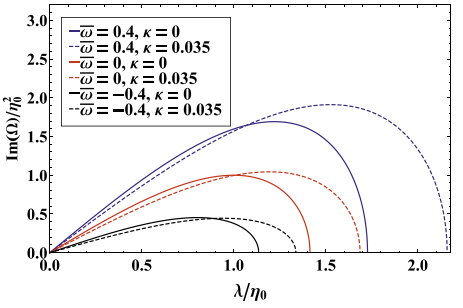

FIGURE 11. Plot of $\mathrm{Im}(\Omega)/\eta_0^2$ as a function of λ/η_0 in deep water for $\overline{v} = 0$ and several values $\overline{\omega}$ and κ.

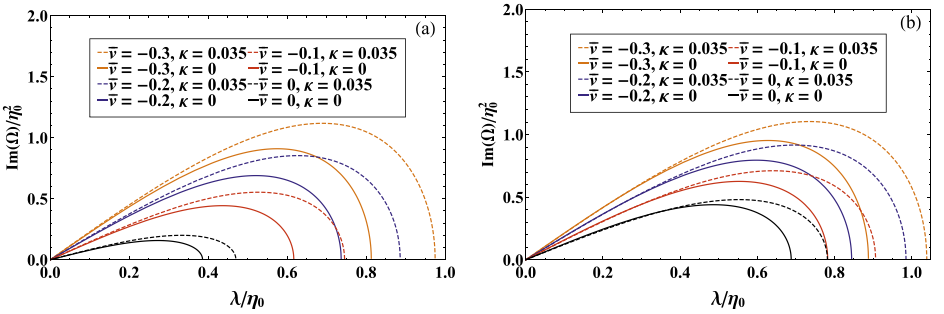

FIGURE 12. Plot of $\mathrm{Im}(\Omega)/\eta_0^2$ as a function of λ/η_0 for $\overline{\omega} = 0$ and several values of $\overline{v}$ and κ: (a) $kd = 1.5$; (b) $kd = 2$.

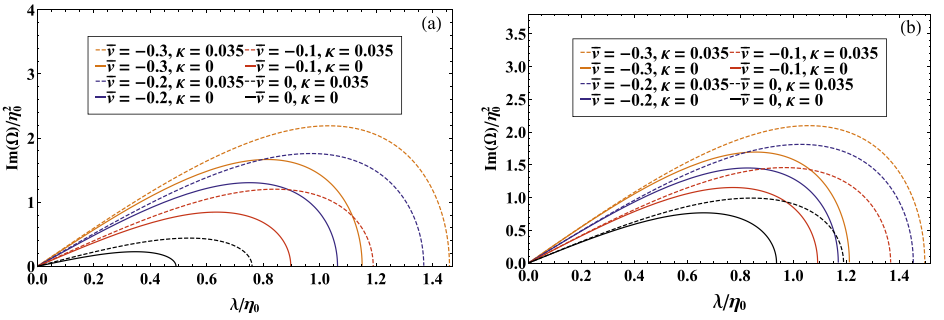

FIGURE 13. Plot of $\mathrm{Im}(\Omega)/\eta_0^2$ as a function of λ/η_0 for $\overline{\omega} = 0.5$ and several values of $\overline{v}$ and κ: (a) $kd = 1.5$; (b) $kd = 2$.

drawn for $\overline{\omega} > -2/3$ and for several values of kd and κ. It is found that for finite depth, the influence of $\overline{\omega}$ is to diminish the maximum growth rate when $-2/3 < \overline{\omega} < 0$, while for $\overline{\omega} > 0$, growth rate first increases with $\overline{\omega}$ and then its value diminishes. For deep water and for $kd = 3.14$, it increases steadily with $\overline{\omega} > 0$. The influence of capillarity is to increase the maximum growth rate for both finite depth and deep water when $\overline{\omega} > 0$.

https://doi.org/10.1017/S1446181123000196 Published online by Cambridge University Press

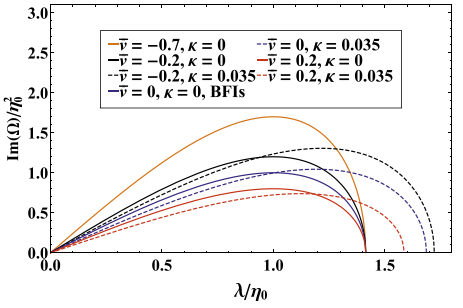

FIGURE 14. Plot of $\mathrm{Im}(\Omega)/\eta_0^2$ as a function of λ/η_0 in deep water for $\overline{\omega} = 0$ and several values $\overline{\nu}$ and κ.

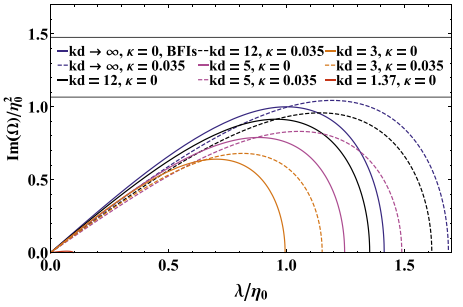

FIGURE 15. Plot of $\mathrm{Im}(\Omega)/\eta_0^2$ as a function of λ/η_0 at several water depths kd for $\overline{\nu} = 0$, $\overline{\omega} = 0$ and $\kappa = 0$, 0.035. BFIs indicates the Benjamin–Feir instability [22] in deep water.

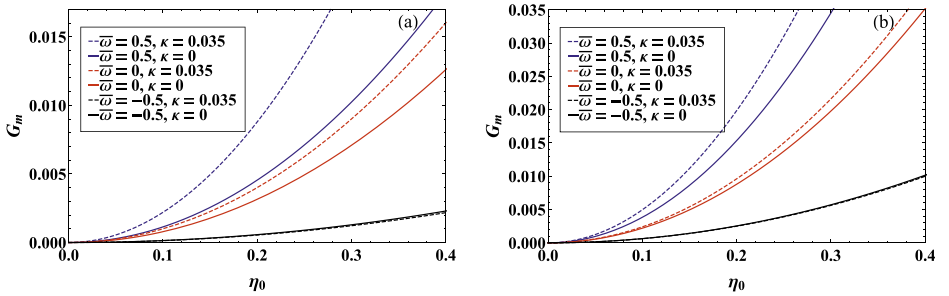

FIGURE 16. Plot of G_m against η_0 for $\overline{\nu} = 0$ and some values of $\overline{\omega}$ and κ: (a) $kd = 1.5$; (b) $kd = 2$.

Furthermore, in Figure 19, we observe first an increase and afterward a decrease of the maximum growth rate for different values of water depth kd.

Figures 20 and 21 show the behaviour of the normalized maximum growth rate of instability against kd. In these cases, the normalization is performed by taking the ratio of the maximum growth rate to its value when $kd \to \infty$. We found from Figure 20 that for $\overline{\omega} \approx 0$, the critical value kd related to re-stabilization is very close to 1.363. Herein, the maximum growth rate increases with the water depth $kd > 1.363$,

https://doi.org/10.1017/S1446181123000196 Published online by Cambridge University Press

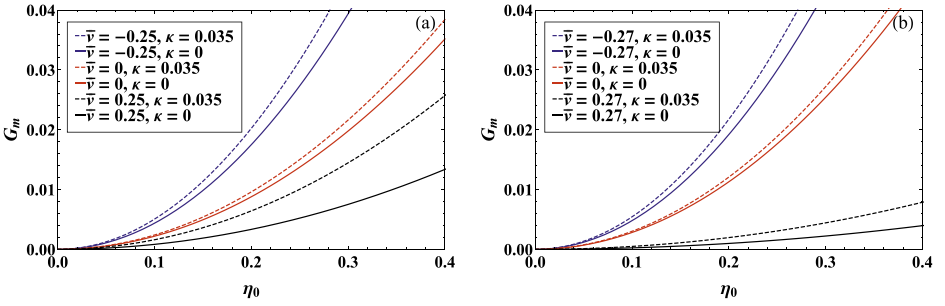

FIGURE 17. Plot of G_m against η_0 for $\overline{\omega} = 0$ and some values of $\overline{\nu}$ and κ: (a) $kd = 2$; (b) $kd = 2.5$.

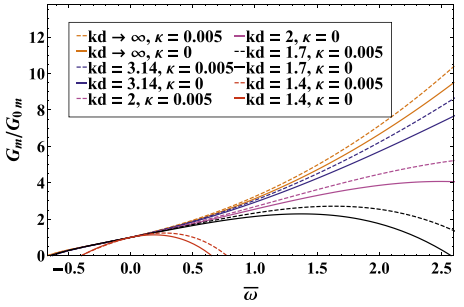

FIGURE 18. Plot of G_m/G_{0m} against $\overline{\omega}$ for $\overline{\nu} = 0$ and some values of kd and κ. Here, G_{0m} represents the maximum growth rate when the shear currents are absent.

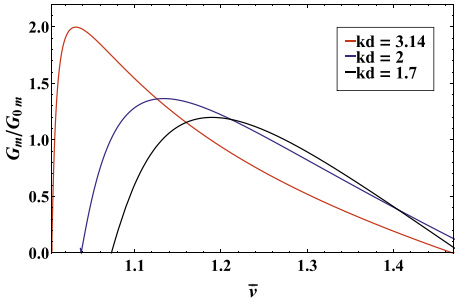

FIGURE 19. Plot of G_m/G_{0m} against $\overline{\nu}$ for $\overline{\omega} = 0$, $\kappa = 0$ and some values of kd. Here, G_{0m} represents the maximum growth rate when the shear currents are absent.

but diminishes with $|\overline{\omega}|$, compatible with the findings of Thomas et al. [39]. Again, Figure 21 shows that depth uniform reverse current increases the maximum growth rate, while following current decreases the growth rate.

The ratio of the normalized instability bandwidth to its value in the absence of shear currents as a function of $\overline{\omega}$ and $\overline{\nu}$ has been plotted respectively in Figures 22 and 23. It is found that for finite depth, the bandwidth of instability BW first increases and then its value decreases with $\overline{\omega}$, while for deep water, its value increases steadily with $\overline{\omega}$.

https://doi.org/10.1017/S1446181123000196 Published online by Cambridge University Press

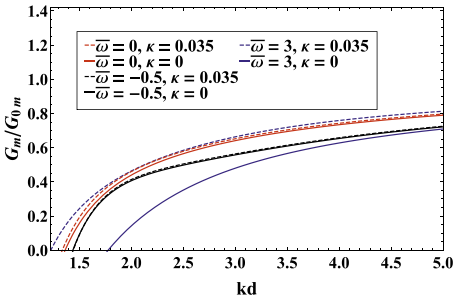

FIGURE 20. Plot of G_m/G_{0m} against kd for $\overline{\nu} = 0$ and some values of $\overline{\omega}$ and κ. Here, G_{0m} represents the maximum growth rate when $kd \to \infty$.

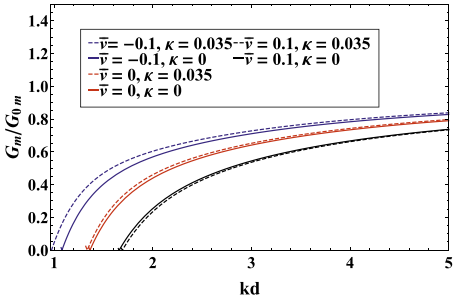

FIGURE 21. Plot of G_m/G_{0m} against kd for $\overline{\omega} = 0$ and some values of $\overline{\nu}$ and κ. Here, G_{0m} represents the maximum growth rate when $kd \to \infty$.

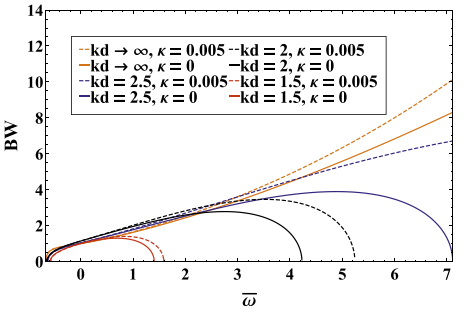

FIGURE 22. Normalized bandwidth of instability against $\overline{\omega}$ for $\overline{\nu} = 0$ and several values of kd and κ.

Moreover, for $\overline{\omega} > 0$, the influence of capillarity shows an increase in the bandwidth for both finite depth and deep water. As found in Figure 22, as described by Thomas et al. [39], our findings without surface tension are in good agreement with the exact numerical results of Oikawa et al. [30]. From Figure 23, we also observe that the instability bandwidth increases with the increase of $\overline{\nu}$ but decreases with the increase of kd.

https://doi.org/10.1017/S1446181123000196 Published online by Cambridge University Press

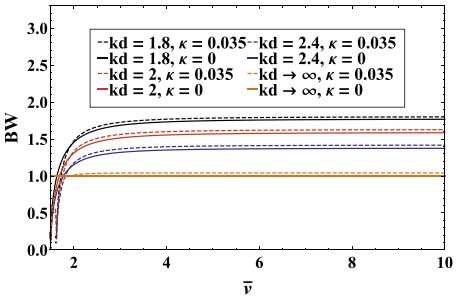

FIGURE 23. Plot of BW against $\overline{v}$ for $\overline{\omega} = 0$ and several values of kd and κ.

5.2. Benjamin–Feir index The concept of the Benjamin–Feir index (BFI) in connection with the random waves was started by Janssen [18] and then elaborated by Onorato et al. [32]. The ratio of the mean square slope to the normalized width of the spectrum is considered as the definition of the BFI. Onorato et al. [33] defined the BFI as

$$\mathrm{BFI} = \frac{\eta_0}{\Delta k}\sqrt{\left|\frac{\mu_1}{\alpha_1}\right|}.$$

Further, the BFI for deep water and for $\overline{\omega} = 0,\ \kappa = 0$ becomes

$$\mathrm{BFI}_0 = \frac{4\eta_0}{\Delta k},$$

where Δk means a typical spectral bandwidth. So the normalized BFI takes the form

$$\mathrm{R} = \frac{\mathrm{BFI}}{\mathrm{BFI}_0} = \frac{1}{4}\sqrt{\left|\frac{\mu_1}{\alpha_1}\right|}. \tag{5.10}$$

Onorato et al. [33] have reported the influence of water depth on the BFI in their figure 1. Thomas et al. [39] have also described the influence of water depth and current shear on the BFI. Herein, we have given attention to the influence of both capillarity and depth uniform current on the BFI. To measure the influence of capillarity on the BFI, we have taken $\overline{\omega} = 0$, $\overline{v} = 0$ in equation (5.10) and then we have portrayed in Figure 24(a) the ratio R of the BFI in the presence of capillarity to its value without capillarity in deep water against kd for several values of κ. It is found that the BFI increases with water depth kd for a fixed value of κ and also the BFI increases with the increase of surface tension κ. For $\kappa = 0$, our results are in good agreement with those of Onorato et al. [33]. The normalized BFI diagram we have obtained is compared in Figure 24(b) with that obtained in figures 11 and 12 of Thomas et al. [39] for $\overline{v} = 0$, $\kappa = 0$. In that way, we can check that this limiting case is again produced accurately. Further, to measure the influence of depth uniform current on the BFI, we have set $\overline{\omega} = 0$, $\kappa = 0$ in equation (5.10) and then we have drawn in Figure 24(c) the ratio R of the BFI with depth uniform current to its value without current as a function of kd. It

https://doi.org/10.1017/S1446181123000196 Published online by Cambridge University Press

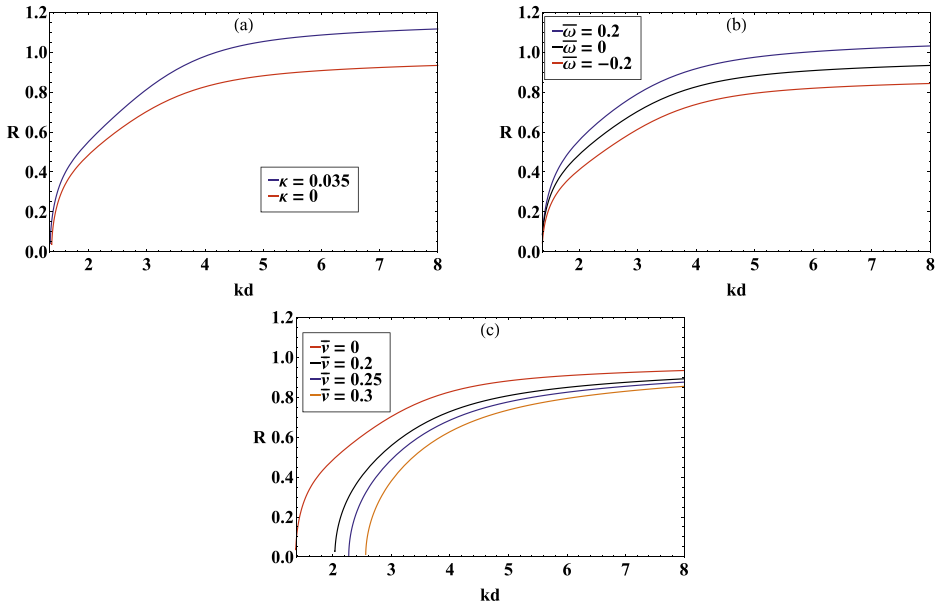

FIGURE 24. Normalized BFI as a function of kd: (a) $\overline{\nu} = 0$, $\overline{\omega} = 0$ and $\kappa = 0,\ 0.035$; (b) $\overline{\nu} = 0$, $\kappa = 0$ and $\overline{\omega} = -0.3,\ 0,\ 1,\ 2$; (c) $\overline{\omega} = 0$, $\kappa = 0$ and $\overline{\nu} = 0,\ 0.2,\ 0.25,\ 0.3$.

is found that the BFI increases with kd for a fixed value of $\overline{\nu}$ but it decreases with the increase of $\overline{\nu}$.

6. Conclusion

In this paper, a higher-order nonlinear evolution equation for gravity-capillary waves in a finite depth of water with linear shear current is developed using the multi-scale expansion. On the basis of the results obtained from both the third- and fourth-order evolution equations, the effect of vorticity, surface tension and depth uniform current on the modulational instability properties of weakly nonlinear gravity-capillary waves are studied. The findings of the present study can be summed up as follows. (i) The main focus is that the new fourth-order results give significant deviations on the instability characteristics compared with the third-order ones and provide better results consistent with the exact results of Longuet-Higgins [24, 25]. (ii) At fourth order, the coefficient $\tilde{\mu}_4$ arises from a nonlinear coupling between wave-induced current and the wave field, and this coupling is still present without current shear. (iii) It is observed that the vorticity significantly modifies the modulational instability and for a finite depth, the combined effect of vorticity and surface tension increases the growth rate considerably in the presence of negative vorticity ($\overline{\omega} > 0$). (iv) For waves moving in the same direction as the depth uniform current, the current is observed to have a stabilizing influence on the waves and reduce the growth

https://doi.org/10.1017/S1446181123000196 Published online by Cambridge University Press

rate of modulational instability. For a uniform reverse current, a rapid destabilization of the waves is predicted in both the cases of finite and infinite depths of water. (v) In deep water, the growth rate of instability decreases up to a certain value of λ, the wavenumber of disturbance, and then it increases due to the effect of capillarity when $\overline{\omega} > 0$. (vi) Finally, it is found that BFI increases with the increase of both the values of surface tension κ and the depth uniform current $\overline{v}$.

Appendix A

The coefficients appearing in the NLEE in equation (3.6) are as follows:

$$\alpha_1 = -\frac{1}{\mu(2-2\overline{v}+\beta)}\Big[\mu(\gamma-\overline{v})^2 + \{p\beta(1-\mu^2)\}\gamma + (1-\overline{v})^2p^2\mu(1-\mu^2) - \{(1-\overline{v})^2+\beta\}p(1-\mu^2) - \frac{(1-\overline{v})(1-\overline{v}+\beta)\kappa}{1+\kappa}\{3\mu+2p(1-\mu^2)\}\Big],$$

$$\alpha_2 = \frac{1}{3(2-2\overline{v}+\beta)}\Big[\frac{1}{2}f_{kkk} - 3\beta p^2(1-\mu^2)\gamma + \{6\gamma + 3(p\overline{\omega}(1-\mu^2) - 2\overline{v})\}\alpha_1\Big],$$

$$\mu_1 = \frac{1}{8\mu^2(1-\overline{v})^2(1-\overline{v}+\beta)(2-2\overline{v}+\beta)} \times \Big[\frac{(P+Q\kappa)(1-\overline{v})}{\mu^2(1-\overline{v}) - \kappa\{(3-\mu^2)(1-\overline{v})+3\beta\}} + S\kappa + \frac{2AB}{C(1+\kappa)}\Big],$$

$$\mu_4 = \frac{(2-2\overline{v}+\beta)}{4\mu^2\{1-(\gamma-\overline{v})\overline{\omega}\}},$$

$$P = (9-12\mu^2+13\mu^4-2\mu^6)(1-\overline{v})^5 + 3(9-6\mu^2+5\mu^4)(1-\overline{v})^4\beta + (33-3\mu^2+4\mu^4)(1-\overline{v})^3\beta^2 + (21+5\mu^2)(1-\overline{v})^2\beta^3 + (7+2\mu^2)(1-\overline{v})\beta^4 + \beta^5,$$

$$Q = (1-\overline{v}+\beta)\{(3-\mu^2)(7-\mu^2)(1-\overline{v})^4 + 2(21+\mu^2-2\mu^4)(1-\overline{v})^3\beta + 2(15+6\mu^2)(1-\overline{v})^2\beta^2 + (9+5\mu^2)(1-\overline{v})\beta^3 + \beta^4\} + 2\{(\mu^2-3)(1-\overline{v}) - 3\beta\} \times \{(4\mu^2-1)(1-\overline{v})^2\beta^2 + (9\mu^2-2)(1-\overline{v})\beta + (6\mu^2-\mu^4-1)\},$$

$$S = 2\mu^2(1-\mu^2)(1-\overline{v})^2 - \{2(1-\mu^2)+3\mu^2/(1+\kappa)\}(1-\overline{v}+\beta)^2,$$

$$A = \{(1-\overline{v}+\beta)^2 - \mu^2(1-\overline{v})^2\}(1+\kappa)(\gamma+p\overline{\omega}) + (1-\overline{v})(1-\overline{v}+\beta)(2-2\overline{v}+\beta),$$

$$B = (\gamma-\overline{v})(1-\mu^2)(1+\kappa) + (1-\overline{v}+\beta)(2-2\overline{v}+\beta),$$

$$C = (\gamma-\overline{v})(\gamma+p\overline{\omega}) - \frac{p(1-\overline{v})(1-\overline{v}+\beta)}{\mu(1+\kappa)},$$

where

$$\gamma = c_g/c = [(1-\overline{v})^2p(1-\mu^2)/\mu + (1-\overline{v})(1-\overline{v}+\beta)(1+3\kappa)/(1+\kappa) + \overline{v}(2-2\overline{v}+\beta)]/(2-2\overline{v}+\beta).$$

https://doi.org/10.1017/S1446181123000196 Published online by Cambridge University Press

Appendix B

The coefficients appearing in equation (4.1) are as follows:

$$\tilde{\alpha}_1 = -\frac{1}{(2-2\overline{\nu}+\overline{\omega})}\left[(\tilde{\gamma}-\overline{\nu})^2 - \frac{3(1-\overline{\nu})(1-\overline{\nu}+\overline{\omega})\kappa}{1+\kappa}\right],$$

$$\tilde{\alpha}_2 = \frac{1}{(2-2\overline{\nu}+\overline{\omega})}[2(\tilde{\gamma}-\overline{\nu})\tilde{\alpha}_1 - \kappa],$$

$$\tilde{\mu}_1 = \frac{1}{8(1-\overline{\nu})^2(1-\overline{\nu}+\overline{\omega})(2-2\overline{\nu}+\overline{\omega})} \times\left[\frac{(\tilde{P}+\tilde{Q}\kappa)(1-\overline{\nu})}{(1-\overline{\nu})-\kappa(2-2\overline{\nu}+3\overline{\omega})} + \frac{\tilde{S}\kappa+2\tilde{A}\tilde{B}/\tilde{C}}{1+\kappa}\right],$$

$$\tilde{\mu}_4 = \frac{(2-2\overline{\nu}+\overline{\omega})}{4\{1-(\tilde{\gamma}-\overline{\nu})\overline{\omega}\}},$$

where

$$\tilde{P} = 8(1-\overline{\nu})^5 + 24(1-\overline{\nu})^4\overline{\omega} + 34(1-\overline{\nu})^3\overline{\omega}^2 + 26(1-\overline{\nu})^2\overline{\omega}^3 + 9(1-\overline{\nu})\overline{\omega}^4 + \overline{\omega}^5,$$

$$\tilde{Q} = (1-\overline{\nu}+\overline{\omega})\{12(1-\overline{\nu})^4 + 40(1-\overline{\nu})^3\overline{\omega} + 42(1-\overline{\nu})^2\overline{\omega}^2 + 14(1-\overline{\nu})\overline{\omega}^3 + \overline{\omega}^4\} - 2\{2(1-\overline{\nu})+3\overline{\omega}\}\{3(1-\overline{\nu})^2\overline{\omega}^2 + 7(1-\overline{\nu})\overline{\omega}+4\},$$

$$\tilde{S} = -3(1-\overline{\nu}+\overline{\omega})^2,$$

$$\tilde{A} = \{(1-\overline{\nu}+\overline{\omega})^2 - (1-\overline{\nu})^2\}(1+\kappa)\overline{\omega},$$

$$\tilde{B} = (1-\overline{\nu}+\overline{\omega})(2-2\overline{\nu}+\overline{\omega}),$$

$$\tilde{C} = (\tilde{\gamma}-\overline{\nu})\overline{\omega} - \frac{(1-\overline{\nu})(1-\overline{\nu}+\overline{\omega})}{(1+\kappa)},$$

$$\tilde{\gamma} = \frac{(1-\overline{\nu})(1-\overline{\nu}+\overline{\omega})(1+3\kappa)}{(2-2\overline{\nu}+\overline{\omega})(1+\kappa)+\overline{\nu}}.$$

Acknowledgements

The authors thank the reviewers for their useful suggestions to improve the manuscript. The Senior Research Fellowship provided by CSIR (India) to Tanmoy Pal is gratefully acknowledged.

References

[1] T. B. Benjamin and J. E. Feir, "The disintegration of wave trains on deep water. Part 1. Theory", *J. Fluid Mech.* **27** (1967) 417–430; doi:10.1017/S002211206700045X.

[2] F. P. Bretherton, C. J. R. Garrett and M. J. Lighthill, "Wavetrains in inhomogeneous moving media", *Proc. R. Soc. Lond. Ser. A* **302** (1968) 529–554; doi:10.1098/rspa.1968.0034.

[3] I. Brevik, "Higher-order waves propagating on constant vorticity currents in deep water", *Coastal Engineering* **2** (1978) 237–259; doi:10.1016/0378-3839(78)90022-4.

https://doi.org/10.1017/S1446181123000196 Published online by Cambridge University Press

[4] U. Brinch-Nielsen and I. G. Jonsson, "Fourth order evolution equations and stability analysis for Stokes waves on arbitrary water depth", *Wave Motion* **8** (1986) 455–472; doi:10.1016/0165-2125(86)90030-2.

[5] W. Choi, "Nonlinear surface waves interacting with a linear shear current", *Math. Comput. Simulation* **80** (2009) 29–36; doi:10.1016/j.matcom.2009.06.021.

[6] A. Constantin, "Two-dimensionality of gravity water flows of constant nonzero vorticity beneath a surface wave train", *Eur. J. Mech. B Fluids* **30** (2011) 12–16; doi:10.1016/j.euromechflu.2010.09.008.

[7] R. A. Dalrymple, "A finite amplitude wave on a linear shear current", *J. Geophys. Res.* **79** (1974) 4498–4504 (1896–1977); doi:10.1029/JC079i030p04498.

[8] A. Davey and K. Stewartson, "On three-dimensional packets of surface waves", *Proc. R. Soc. Lond. Ser. A.* **338**(1613) (1974) 101–110; doi:10.1098/rspa.1974.0076.

[9] A. K. Dhar and J. T. Kirby, "Fourth-order stability analysis for capillary-gravity waves on finite depth currents with constant vorticity", *Phys. Fluids* **35** (2023) Article ID: 026601; doi:10.1063/5.0136002.

[10] V. D. Djordjevic and L. G. Redekopp, "On two-dimensional packets of capillary-gravity waves", *J. Fluid Mech.* **79** (1977) 703–714; doi:10.1017/S0022112077000408.

[11] K. B. Dysthe, "Note on a modification to the nonlinear Schrödinger equation for application to deep water waves", *Proc. R. Soc. Lond., Ser. A* **369**(1736) (1979) 105–114; doi:10.1098/rspa.1979.0154.

[12] W. J. Harrison, "The influence of viscosity and capillarity on waves of finite amplitude", *Proc. Lond. Math. Soc.* s**2–7**(1) (1909) 107–121; doi:10.1112/plms/s2-7.1.107.

[13] K. B. Hjelmervik and K. Trulsen, "Freak wave statistics on collinear currents", *J. Fluid Mech.* **637** (2009) 267–284; doi:10.1017/S0022112009990607.

[14] S. J. Hogan, "The fourth-order evolution equation for deep-water gravity-capillary waves", *Proc. R. Soc. Lond. Ser. A* **402**(1823) (1985) 359–372; doi:10.1098/rspa.1985.0122.

[15] H.-C. Hsu, M. Francius, P. Montalvo and C. Kharif, "Gravity–capillary waves in finite depth on flows of constant vorticity", *Proc. R. Soc. Lond. Ser. A* **472**(2195) (2016), Article ID: 20160363; doi:10.1098/rspa.2016.0363.

[16] H. C. Hsu, C. Kharif, M. Abid and Y. Y. Chen, "A nonlinear Schrödinger equation for gravity–capillary water waves on arbitrary depth with constant vorticity. Part 1", *J. Fluid Mech.* **854** (2018) 146–163; doi:10.1017/jfm.2018.627.

[17] Z. Huang and C. C. Mei, "Effects of surface waves on a turbulent current over a smooth or rough seabed", *J. Fluid Mech.* **497** (2003), 253–287; doi:10.1017/S0022112003006657.

[18] P. A. E. M. Janssen, "On a fourth-order envelope equation for deep-water waves", *J. Fluid Mech.* **126** (1983) 1–11; doi:10.1017/S0022112083000014.

[19] R. S. Johnson and K. Stewartson, "On the modulation of water waves on shear flows", *Proc. R. Soc. Lond. Ser. A* **347**(1651) (1976) 537–546; doi:10.1098/rspa.1976.0015.

[20] I. Kantardgi, "Effect of depth current profile on wave parameters", *Coastal Engineering* **26** (1995) 195–206; doi:10.1016/0378-3839(95)00021-6.

[21] N. Kishida and R. J. Sobey, "Stokes theory for waves on linear shear current", *J. Eng. Mech.* **114** (1988) 1317–1334; doi:10.1061/(ASCE)0733-9399(1988)114:8(1317).

[22] B. Liao, G. Dong, Y. Ma and J. L. Gao, "Linear-shear-current modified Schrödinger equation for gravity waves in finite water depth", *Phys. Rev. E* **96** (2017) Article ID 043111; doi:10.1103/PhysRevE.96.043111.

[23] P. L.-F. Liu, M. W. Dingemans and J. K. Kostense, "Long-wave generation due to the refraction of short-wave groups over a shear current", *J. Phys. Oceanogr.* **20** (1990) 53–59; doi:10.1175/1520-0485(1990)020<0053:LWGDTT>2.0.CO;2.

[24] M. S. Longuet-Higgins, "The instabilities of gravity waves of finite amplitude in deep water II. Subharmonics", *Proc. R. Soc. Lond. Ser. A* **360**(1703) (1978) 489–505; doi:10.1098/rspa.1978.0081.

[25] M. S. Longuet-Higgins and R. W. Stewart, "The changes in amplitude of short gravity waves on steady non-uniform currents", *J. Fluid Mech.* **10** (1961) 529–549; doi:10.1017/S0022112061000342.

https://doi.org/10.1017/S1446181123000196 Published online by Cambridge University Press

[26] Y. Ma, X. Ma, M. Perlin and G. Dong, "Extreme waves generated by modulational instability on adverse currents", *Phys. Fluids* **25** (2013) Article ID: 114109; doi:10.1063/1.4832715.
[27] R. D. MacIver, R. R. Simons and G. P. Thomas, "Gravity waves interacting with a narrow jet-like current", *J. Geophys. Res.: Oceans* **111**(C3) (2006) C03009; doi:10.1029/2005JC003030.
[28] L. F. McGoldrick, "On Wilton's ripples: a special case of resonant interactions", *J. Fluid Mech.* **42** (1970) 193–200; doi:10.1017/S0022112070001179.
[29] C. C. Mei and E. Lo, "The effects of a jet-like current on gravity waves in shallow water", *J. Phys. Oceanogr.* **14** (1984) 471–477; doi:10.1175/1520-0485(1984)014<0471:TEOAJL>2.0.CO;2.
[30] M. Oikawa, K. Chow and D. J. Benney, "The propagation of nonlinear wave packets in a shear flow with a free surface", *Stud. Appl. Math.* **76** (1987) 69–92; doi:10.1002/sapm198776169.
[31] M. Okamura and M. Oikawa, "The linear stability of finite amplitude surface waves on a linear shearing flow", *J. Phys. Soc. Japan* **58** (1989) 2386–2396; doi:10.1143/JPSJ.58.2386.
[32] M. Onorato, A. R. Osborne, M. Serio and S. Bertone, "Freak waves in random oceanic sea states", *Phys. Rev. Lett.* **86** (2001) 5831–5834; doi:10.1103/PhysRevLett.86.5831.
[33] M. Onorato, A. R. Osborne, M. Serio, L. Cavaleri, C. Brandini and C. T. Stansberg, "Extreme waves, modulational instability and second order theory: wave flume experiments on irregular waves", *Eur. J. Mech. B Fluids* **25** (2006) 586–601. doi:10.1016/j.euromechflu.2006.01.002.
[34] O. S. Pak and K. W. Chow, "Free surface waves on shear currents with non-uniform vorticity: third-order solutions", *Fluid Dyn. Res.* **41** (2009) Article ID: 035511; doi:10.1088/0169-5983/41/3/035511.
[35] D. H. Peregrine, "Interaction of water waves and currents", *Adv. Appl. Mech.* **16** (1976) 9–117; doi:10.1016/S0065-2156(08)70087-5.
[36] Y. V. Sedletsky, "The modulational instability of Stokes waves on the surface of finite-depth fluid", *Phys. Lett. A* **343** (2005) 293–299; doi:10.1016/j.physleta.2005.04.076.
[37] J. Simmen and P. G. Saffman, "Steady deep-water waves on a linear shear current", *Stud. Appl. Math.* **73** (1985) 35–57; doi:10.1002/sapm198573135.
[38] A. F. Teles da Silva and D. H. Peregrine, "Nonlinear perturbations on a free surface induced by a submerged body: a boundary integral approach", *Eng. Anal. Bound. Elem.* **7** (1990) 214–222; doi:10.1016/0955-7997(90)90007-V.
[39] R. Thomas, C. Kharif and M. Manna, "A nonlinear Schrödinger equation for water waves on finite depth with constant vorticity", *Phys. Fluids* **24** (2012) Article ID: 127102; doi:10.1063/1.4768530.
[40] S. Tsao, "Behaviour of surface waves on a linearly varying flow", *Tr. Mosk. Fiz.-Tekh. Inst. Issled. Mekh. Prikl. Mat.* **3** (1959) 66–84.
[41] J. R. Wilton, "On ripples", *London, Edinburgh, Dublin Philos. Mag. J. Sci.* **29** (1915) 688–700; doi:10.1080/14786440508635350.
[42] H. C. Yuen and B. M. Lake, "Nonlinear deep water waves: theory and experiment", *Phys. Fluids* **18** (1975) 956–960; doi:10.1063/1.861268.

https://doi.org/10.1017/S1446181123000196 Published online by Cambridge University Press